

# River Routing in the INM RAS-MSU Land Surface Model: Numerical Scheme and Parallel Implementation on Hybrid Supercomputers

Victor M. Stepanenko<sup>1,2</sup> 

© The Author 2022. This paper is published with open access at SuperFri.org

The land surface model (LSM) is a necessary compartment of any numerical weather forecast system or the Earth system model. This paper presents a new version of the INM RAS-MSU land surface model where the river hydrodynamic and thermodynamic scheme is embedded into the parallel execution framework using MPI and OpenMP. Numerical experiments have been performed for the East European domain with resolution  $0.5^\circ \times 0.5^\circ$ . The soil model parallel efficiency at 1–144 MPI cores was 0.52–0.79 and limited by the presence of ocean area, and by imbalance of computational load between soil columns. The acceleration of the river model at MPI level was defined by the size of the largest river basin in the domain. At the OpenMP level, the potential for acceleration of large river basin simulation is shown to be close to number of threads used, based on fractal properties of the river networks. This acceleration was hindered in our numerical experiments by the reduced river orders at the coarse land surface model resolution, so that the optimal speedup for the Volga river basin was 2.5–3 times attained at 4–6 threads. This performance is projected to improve with refinement of the LSM spatial resolution.

*Keywords:* land surface model, soil, river network, MPI, OpenMP.

## Introduction

The land surface scheme (or land surface model, LSM) is a necessary compartment of any numerical weather forecast system or the Earth system model. It reproduces the thermodynamic, hydrophysical and ecological state of land active layer as well as momentum, mass and energy fluxes between Earth surface and the atmosphere. These fluxes are important to reproduce well for reliable weather forecasts at a broad range of time scales: from subdiurnal to seasonal. Especially, the soil moisture is widely recognized as a critical parameter for seasonal weather dynamics and prediction [6, 19, 32], as it defines the structure of the soil surface heat balance.

Rivers are an integrating component of the land water cycle, as they gather soil moisture from large terrestrial areas and transport it to ocean. The significance of rivers in the Earth system is caused by their notable contribution to the ocean freshwater budget [14, 23], methane, carbon dioxide [17, 21, 29] and dissolved organic carbon [2, 3] transfer from land to ocean and emission of greenhouse gases to the atmosphere. In addition, the river discharge at large timescales is close to accumulated “precipitation minus evaporation” over the river basin, and thus serves as a useful proxy for this difference during the land surface model validation. Those considerations led to introduction to the land surface models the so-called river routing schemes representing river flows in simplified manner [1, 11, 15, 22, 31].

The land surface models for long have been consisting of a large number of independent vertical 1D soil problems, enabling straightforward parallel implementation using MPI and the longitude-latitude domain decomposition technique. However, embedding river module introduces horizontal dependency of river variables and thus existing longitude-latitude decomposition is not optimal for LSM river module. This calls for development of new parallel implementation

---

<sup>1</sup>Lomonosov Moscow State University, Moscow, Russian Federation

<sup>2</sup>Moscow Center of Fundamental and Applied Mathematics, Moscow, Russian Federation

approach to LSMs with advanced river simulators. Our paper addresses this objective for the INM RAS-MSU land surface scheme.

The paper is organized as follows. Section 1 presents general information on the INM RAS-MSU model basic equations and physical parameterizations, with detailed description of the soil module. Section 1.2 is devoted to the recently developed thermo- and hydrodynamic model of the river network inside INM RAS-MSU LSM. Information structure of the INM RAS-MSU simulator with river block is elaborated in Section 2; the corresponding levels of parallelism are analyzed in Section 3. Configuration of numerical experiments with parallelized LSM is described in Section 4. Results of experiments are demonstrated and discussed in Section 5. Conclusions summarize key results of the study, and sketch future directions for the optimization of LSM parallel implementation.

## 1. The INM RAS-MSU Land Surface Scheme

The land surface scheme used in this study is jointly developed by Institute of Numerical Mathematics (INM), Russian Academy of Sciences, and Lomonosov Moscow State University (MSU) (Fig. 1). It is a part of the INM-CM5 Earth system model [27] and of the SL-AV numerical weather forecast system [10]. Here, we consider it in a standalone version, where the atmospheric forcing is prescribed. It reproduces the thermodynamic and hydrophysical state of soil, lakes and rivers as well as momentum, mass and energy fluxes between Earth surface and the atmosphere. The effects of surface vegetation on surface-atmosphere exchanges are represented via modifications of soil-air exchange laws (based mostly on Monin-Obukhov similarity) and introduction of liquid water sink in soil due to roots suction. This means, no vegetation layer storage for heat or mass is considered. Subgrid-scale variability of the land surface is simulated by tile approach, where contribution of each surface type in a cell to cell-averaged fluxes of heat, radiation, water vapor and carbon is proportional to its areal fraction. Carbon cycle processes accounted for into the model include photosynthesis, organic matter decay in soils with CO<sub>2</sub> release and organics degradation in wetlands with CH<sub>4</sub> formation. The most computationally expensive parts of INM RAS-MSU land model are soil, lake and river modules. The soil and river modules are described in more detail below. The lake model is similar in its information structure to the soil model, as both of them comprise a number of independent 1D problems.

### 1.1. Soil Model

The basic numerical kernel of any land surface scheme is a solver for an equation system describing heat and water transport in soil and snow, including phase transitions. In INM RAS-MSU model, this system includes equations as follows. The heat equation is:

$$\rho_d c \frac{\partial T}{\partial t} = \frac{\partial}{\partial z} \lambda_T \frac{\partial T}{\partial z} + \rho_d (L_i F_i - L_v F_v), \quad (1)$$

where  $\rho_d c$  is a volumetric heat capacity of soil,  $T$  is temperature,  $z$  is a coordinate directed along acceleration due to gravity,  $t$  is time,  $\lambda_T$  is coefficient of heat conductivity,  $\rho_d$  is dry soil bulk density,  $L_k$  and  $F_k$  are the specific heat and rate of water freezing/melting ( $k = i$ ) and evaporation/condensation ( $k = v$ ), respectively. The heat conductivity  $\lambda_T$  is a function of liquid water content  $W$  and dry soil conductivity. An equation for liquid water content  $W$  describes vertical transport (diffusion due to capillary and sorption forces and gravitational infiltration),

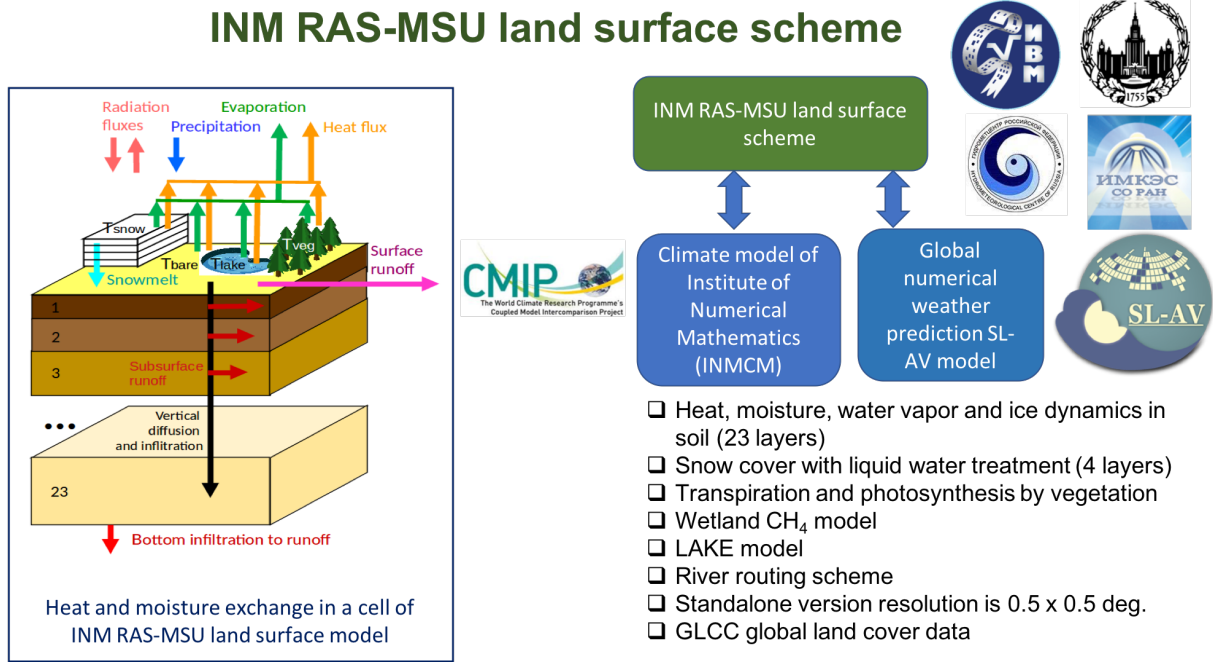


**Figure 1.** INM RAS-MSU land surface model

freezing/melting and evaporation/sublimation, root uptake and horizontal discharge [16]:

$$\frac{\partial W}{\partial t} = \frac{\partial}{\partial z} \left( \lambda_W \frac{\partial W}{\partial z} + \lambda_I \frac{\partial I}{\partial z} \right) + \frac{\partial \gamma}{\partial z} - F_i - F_v - S_r - S_l. \quad (2)$$

Here,  $W$  is a ratio of liquid water mass to solid soil matrix mass,  $S_r$  is root suction, and  $S_l$  is a sink due to lateral water flow. A dependence of soil moisture potential  $\Psi$  (or water retention curve, WTC) and hydraulic conductivity  $\gamma$  on moisture  $W$  and ice content  $I$  are important features of the system, defining coefficients  $\lambda_W, \lambda_I, \gamma$  as functions of the solution ( $\lambda_I$  is neglected in the current version of the model). The liquid water diffusivity  $\lambda_W(W)$  and hydraulic conductivity  $\gamma(W)$  are related functions:

$$\lambda_W(W) = \gamma(W) \frac{\partial \Psi(W)}{\partial W}. \quad (3)$$

At least 22 semi-empirical forms are proposed for WTC [9], fitting different sets of empirical data with different performance. The WTC function explicitly enters the hydraulic conductivity function  $\gamma$ . For instance, choosing Mualem approach for hydraulic conductivity quantification [20], one gets:

$$\gamma = \gamma_{max} \widetilde{W}^{1/2} \left[ \int_0^{\widetilde{W}} \frac{d\widetilde{W}'}{\Psi(\widetilde{W}')} \left( \int_0^1 \frac{d\widetilde{W}'}{\Psi(\widetilde{W}')} \right)^{-1} \right]^2, \quad (4)$$

where  $\widetilde{W} \doteq (W - W_{min}) / (W_{max} - W_{min})$  is a degree of soil moisture saturation. Thus, introducing in (4) and (3) different forms of WTC yields corresponding pairs of functions  $(\lambda_W, \gamma)$ , based on Mualem equation. In INM RAS-MSU model, the two most widespread sets of  $(\lambda_W, \gamma)$  are implemented, namely those by Brooks-Corey [4, 5] and Mualem-van Genuchten [12, 20].

The content of water vapor ( $V$ , expressed as a mass ratio, similar to  $W$ ) is governed by diffusion equation and phase transitions:

$$\frac{\partial V}{\partial t} = \frac{\partial}{\partial z} \lambda_V \frac{\partial V}{\partial z} + F_v, \quad (5)$$

while the dynamics of ice content  $I$  is defined by phase transitions only:

$$\frac{\partial I}{\partial t} = F_i. \quad (6)$$

The system of four equations above is supplemented by boundary conditions, representing heat and water mass balance at the soil-air interface  $z = 0$  and the bottom of soil column  $z = H$ . At the surface, heat and water balance equations include net radiation and modification of fluxes by vegetation canopy, while at bottom zero diffusive flux condition is imposed. In cold season, snow depth dynamics is simulated as well as temperature and snow moisture vertical distribution [24, 28]:

$$\rho_{sn} c_{sn} \frac{\partial T}{\partial t} = \frac{\partial}{\partial z} \lambda_T \frac{\partial T}{\partial z} + \rho_{sn} L_i F_i, \quad (7)$$

$$\frac{\partial W}{\partial t} = \frac{\partial \gamma}{\partial z} - F_i, \quad (8)$$

where the subscript ‘‘sn’’ denotes thermodynamic properties of snow. This system is coupled to the soil equations set via continuity of fluxes and temperature at the soil-snow interface.

The system is solved by implicit in time and central-differences in space numerical scheme with 23 levels in soil down to 10 m depth, 4 levels in snow (if present) and 1 hour time step for every cell of a regular latitude-longitude grid ( $0.5^\circ \times 0.5^\circ$  in this study). In order to ensure the heat balance equation at the soil surface, iteration procedure in respect to surface temperature is implemented.

The code is written in Fortran and uses the external libraries for I/O in netcdf format, MPI exchanges and OpenMP threading.

## 1.2. The Model for River Hydrodynamics and Thermodynamics

The model for river hydrodynamics and thermodynamics is based on diffusive wave approximation for 1D (i.e. averaged over the vertical cross-section of a stream) Saint-Venant system [24]. Under this approach, the pressure gradient force is balanced by quadratic bottom friction, which delivers a closed set of equations for vertical cross-section area  $S$  and temperature  $T$ :

$$\frac{\partial S}{\partial t} + \frac{\partial([U_0 + U_*]S)}{\partial x} = E_r + \frac{\partial}{\partial x} k_S \frac{\partial S}{\partial x}, \quad (9)$$

$$\frac{\partial(ST)}{\partial t} + \frac{\partial([U_0 + U_*]ST)}{\partial x} = u_{tr} T_{tr} h_{tr} + b_s F + \frac{\partial}{\partial x} k_{ST} \frac{\partial S}{\partial x}, \quad (10)$$

supplemented with boundary conditions:

$$S|_{x=0} = \frac{\partial S}{\partial x} \Big|_{x=L} = 0, \quad (11)$$

$$ST|_{x=0} = 0, \quad (12)$$

where the along-river coordinate  $x = 0$  corresponds to the river origin and  $x = L$  locates at the river mouth,  $E_r$  is a water volume inflow rate from soil and tributaries per unit of river length,  $u_{tr} T_{tr} h_{tr}$  is heat inflow per river unit length from soil and inlets,  $b_s$  is a width of a river surface,  $F$  is net kinematic heat and radiation flux at the water surface,  $U_*$ ,  $k_S$  and  $k_{ST}$  are functions of channel slope and geometry. The net radiation includes shortwave and longwave components, net heat flux includes sensible and latent heat flux calculated by the same Monin-Obukhov similarity as for the soil model (with water-specific roughness lengths). The ice cover

is not explicitly simulated in the current version, and water temperature is allowed to decrease below 0°C.

The system is solved for each river by Preisman scheme semi-implicit in time with 10 mesh nodes per the model cell (Fig. 2) and Vreman conservative filtering [30] to suppress two-step oscillations.

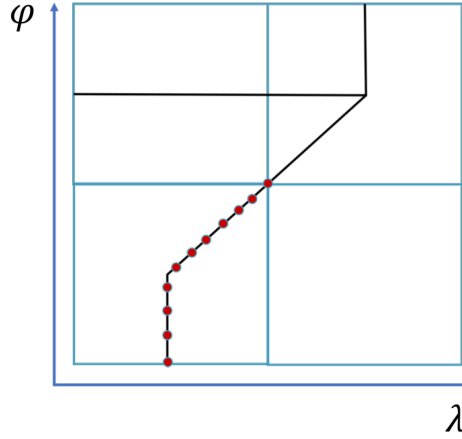


**Figure 2.** The nodes of the river numerical scheme (red circles on a black line, the black line representing river course) on a grid of land surface model (blue rectangles),  $\lambda$  is longitude,  $\phi$  is latitude (adopted from [24])

## 2. Information Structure of the Land Surface Model with River Routing

The soil and river models are one-way coupled. It means that the solution of the soil problem affects the solution of the river model (via groundwater runoff), but not vice versa. The total water volume source in the stream continuity equation (9) is  $E_r = E_{r,s} + E_{r,r}$ , where  $E_{r,s}$  is the soil runoff, and  $E_{r,r}$  is the water input from tributaries. The soil water runoff to rivers in each model cell is:

$$E_{r,s} = \frac{A}{\rho_{w0}L_A} \left[ (\rho_d \gamma) |_{z=H} + \int_0^H \rho_d S_l dz \right], \quad (13)$$

where  $A$  is a cell area,  $L_A$  is a total river length in a cell, and  $\rho_{w0}$  is the reference water density. Thus, an update of soil variables in a cell during timestep provides  $E_{r,s}$  over this time step to be used in a river model as a longitude-latitude field. The water input from tributaries  $E_{r,r}$  is:

$$E_{r,r} = [(U_0 + U_*)S]_{tr}/L_A, \quad (14)$$

with subscript “tr” denoting the tributary(ies) of the river, if any in the cell. The heat source in (10) is:

$$u_{tr}T_{tr}h_{tr} = E_{r,s}H_a^{-1} \int_0^{H_a} T dz + [(U_0 + U_*)ST]_{tr}/L_A, \quad (15)$$

with  $H_a$  standing for active soil layer depth, assumed 1 m in current model version. The above formulas mean that in order to advance river variables at each time step the soil runoff and discharge of tributaries are necessary. Thus the sequence of model execution at each time step is as follows (omitting other parts of algorithm such as lakes, I/O, etc.):

- soil model (time step  $i$ ),
- river model (time step  $i$ ):
  - rivers of the 1st order,
  - rivers of the 2nd order,
  - ...
  - rivers of the maximal order.
- soil model (time step  $i + 1$ ),
- river model (time step  $i + 1$ ):
  - rivers of the 1st order,
  - ...

Here, we introduced the Strahler orders of rivers, where by definition, rivers of order  $n$  have tributaries of the order not larger than  $n - 1$ , and the streams having no inlets are of  $n = 1$ . This is the strict sequence that cannot be changed under selected numerical scheme. The independent in terms of information exchange parts of the algorithm are:

- time step updates of different soil columns,
- time step updates of different river basins,
- time step updates of different rivers of the same order.

Here, we used a term “basin” to denote a river network with highest-order river flowing into the ocean or a lake with no outlet. The serial and parallel parts of the algorithm indicated above cause the levels of parallel implementation described in the following section.

The INM RAS-MSU land surface model with river routine scheme described above was shown to successfully reproduce the annual cycle of runoff of two North Eurasian rivers: Severnaya Dvina and Kolyma [18, 24].

### 3. Levels of Parallelism and Analytical Estimates for Model Speedup

The soil model is parallelized using standard decomposition of longitude-latitude domain in  $M_\lambda M_\phi$  subdomains of the same dimensions, where  $M_\lambda$  and  $M_\phi$  are the numbers of MPI processes along those two coordinates, respectively. Given no data exchanges are needed between any two MPI processes for soil simulations, this part of the model should speedup with efficiency  $\approx 1$  under even computational load of processes.

The river model parallel implementation consists of two levels. The top level comprises the distribution of river basins between MPI processes. This distribution is realized as follows. Let us assume, there are  $N_b$  basins in the model domain, and  $n_i$ ,  $i = 1, \dots, N_b$  is a decreasing sequence of numbers of land model cells constituting these basins. Then, the MPI process of rank 0 simulates the largest basin ( $i = 1$ ), whereas  $k$ -th process computes dynamics of rivers in basins labeled  $i = i_{1,k}, \dots, i_{m_k,k}$ , so that the total number of cells in those basins  $\sum_{i=i_{1,k}, \dots, i_{m_k,k}} n_i \leq n_1$ , and closest possible to  $n_1$ . Such a scheme ensures distribution of basins between a small number of MPI processes which is even in terms of total number of land model cells, but not necessarily in number of basins.

To supply the river model with input data (meteorological variables, inflow of water volume and heat from soil to streams), each MPI process should have access to the 2D (lan-lot) arrays of those variables covering all river basins, which are associated to this process. However, these 2D arrays are originally split between MPI-processes according to 2D domain decomposition of

the soil model (see the first paragraph of this Section, and Fig. 5 in Section 4). This issue is solved by allocating auxiliary 2D array covering the whole simulation domain which is identical on each MPI process and which is filled in with the above mentioned variables by ALLREDUCE operation. This operation is performed one time each time step after the call of soil update (PBLFLX subroutine) and before the river update (RIVWAT subroutine).

The second level of parallelizm of the river model is realized for each MPI process, and uses the informational independency of river equations solution for rivers of the same order. This level is implemented using OpenMP instructions. Below we estimate the maximal speedup for a single river basin simulation following this approach, which is attainable under no overhead costs.

Let  $\omega$  be the Strahler order of a river. We can now introduce the values  $n_\omega$  (total number of watercourses of order  $\omega$  in a given basin) and  $L_\omega$  (average length of watercourses of order  $\omega$  in the basin). According to Horton's laws, which can be derived from an approximation that the river network is a fractal [8, 25], the following relations are statistically valid:

$$\frac{n_{\omega-1}}{n_\omega} = C_n > 1, \quad (16)$$

$$\frac{L_{\omega-1}}{L_\omega} = C_L < 1, \quad (17)$$

where  $C_n$  and  $C_L$  are constants of the river basin. The wall-clock time of solving a one-dimensional problem for one river at one time step can be expressed as  $O(L_\omega^k)$ , where  $k$  is defined by numerical scheme, e.g.,  $k = 1$  for explicit schemes and implicit schemes, where linear systems are solved by direct factorization method (the case of our model). Now estimate the time of sequential processing  $T_s$ , i.e., time needed for sequential solution of one-dimensional problems for all rivers of the river basin. For the number of rivers of order  $\omega$  and their length we have:

$$n_\omega = n_{\omega-1}C_n^{-1} = \dots = n_1C_n^{-(\omega-1)}, \quad (18)$$

$$L_\omega = L_{\omega-1}C_L^{-1} = \dots = L_1C_L^{-(\omega-1)}. \quad (19)$$

Let  $\omega_{max}$  be a maximal order of rivers in the basin. Then

$$T_s = \sum_{\omega=1}^{\omega_{max}} n_\omega O(L_\omega^k) = n_1 O(L_1^k) \sum_{\omega=1}^{\omega_{max}} C_L^{-k(\omega-1)} C_n^{-(\omega-1)}. \quad (20)$$

Since  $1 = n_{\omega_{max}} = n_1 C_n^{-(\omega_{max}-1)}$ , and introducing  $C_L^* \doteq C_L^{-1} > 1$ , the expression for  $T_s$  reads:

$$T_s = C_n^{\omega_{max}-1} O(L_1^k) \sum_{\omega=0}^{\omega_{max}-1} C_n^{-\omega} C_L^{*k\omega}. \quad (21)$$

If all rivers of the same order are processed simultaneously by different cores, then the update of all rivers of order  $\omega$  takes the time  $O(L_\omega^k)$  rather than  $n_\omega O(L_\omega^k)$  as in the sequential version, so that the total processing time of the whole river network  $T_p$  is estimated as:

$$T_p = O(L_1^k) \sum_{\omega=0}^{\omega_{max}-1} C_L^{*k\omega}, \quad (22)$$

and the speedup of the whole river basin simulation:

$$\frac{T_s}{T_p} = \frac{C_n^{\omega_{max}-1} \sum_{\omega=0}^{\omega_{max}-1} C_n^{-\omega} C_L^{*k\omega}}{\sum_{\omega=0}^{\omega_{max}-1} C_L^{*k\omega}}. \quad (23)$$

If for the river basin processing only  $m$  cores are available, the above estimate transforms to:

$$\frac{T_s}{T_p} = \frac{\sum_{\omega=0}^{\omega_{max}-1} C_n^{\omega_{max}-\omega-1} C_L^{*k\omega}}{\sum_{\omega=0}^{\omega_{max}-1} \max [C_n^{\omega_{max}-\omega-1} / m, 1] C_L^{*k\omega}}. \quad (24)$$

An example of river model speedup for single basin processing according to (24) is shown in Fig. 3. One can see that for largest river basins (with maximal river order exceeding 6–8) the speedup approaches the number of cores used. This is important, as the largest basins cause a bottleneck at the MPI level of river model implementation, and their effective speedup at the OpenMP level may significantly reduce the execution time of the whole river module.

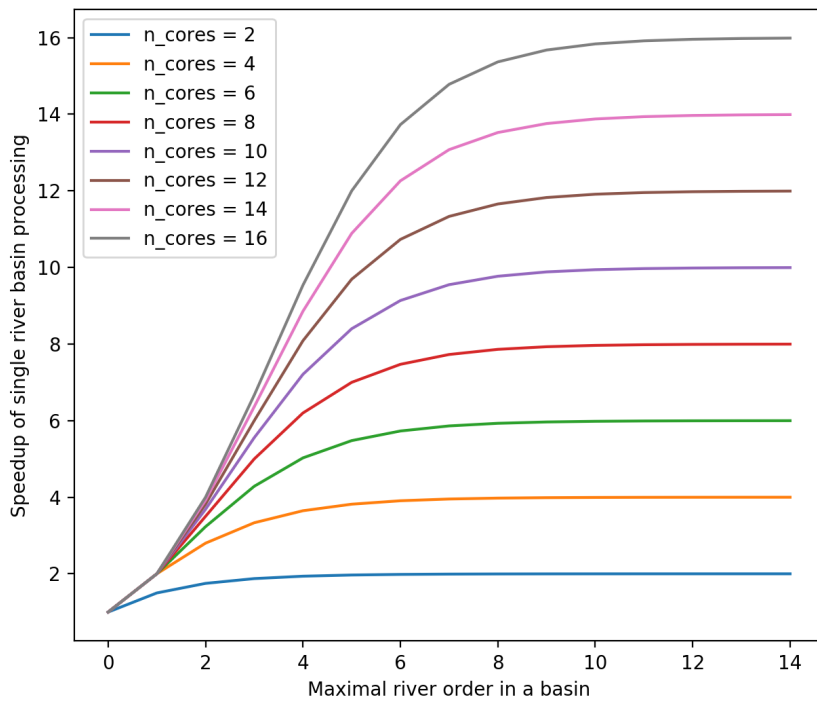


**Figure 3.** Theoretical speedup of a single river basin processing with no overhead costs, as estimated from fractal theory ( $C_n = 4$ ,  $C_L^* = 2$ )

## 4. Configuration of Numerical Experiments

Numerical experiments with INM RAS-MSU land surface model have been conducted for domain 40°–80° N, 20°–59.5° E with horizontal resolution 0.5° × 0.5° and for the period of 31 days. Atmospheric forcing (surface air temperature, humidity, wind speed, downwelling longwave and shortwave radiation, pressure, precipitation) was read from GFDL-ESM2M piControl simulation data, 1–31 Jan 1661, bias-corrected EWEMBI dataset of the ISIMIP2b project (<https://www.isimip.org>). Atmospheric data has the same grid with the model, temporal resolution is daily, the model time step is 1 hour. The data for river flow directions and riverbed slopes are taken from the database of GWSP-WATCH project based on DDM30 data [7] made accessible through ISIMIP project as well. The resulting river network of the Volga basin is shown in Fig. 5. On

the model mesh, Volga river has the order 6, which is much less than that defined for the river network obtained at much finer resolution (the Volga order is 9 at 200–500 m resolution, [13]).

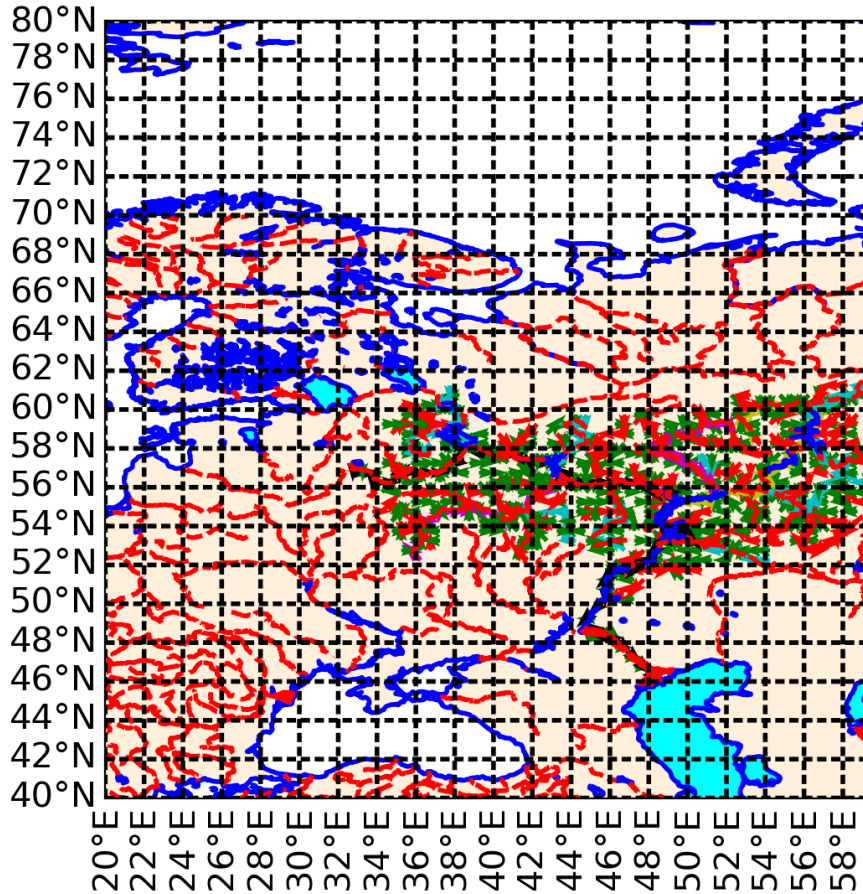


**Figure 4.** The full domain of the INM RAS-MSU land surface model simulations. The small green arrows depict the Volga river basin, shown in detail in Fig. 5

Two series of experiments have been performed to measure the model speedup:

- MPI series: 1 OpenMP thread, number of MPI processes: 1, 4 ( $M_\lambda = M_\phi = 2$ ), 16 ( $M_\lambda = M_\phi = 4$ ), 36 ( $M_\lambda = M_\phi = 6$ ), 64 ( $M_\lambda = M_\phi = 8$ ), 100 ( $M_\lambda = M_\phi = 10$ ), 144 ( $M_\lambda = M_\phi = 12$ ),
- OpenMP series: 4 MPI processes ( $M_\lambda = M_\phi = 2$ ), number of OpenMP threads: 1, 2, 4, 6, 8, 10, 12, 14.

The performance of the model at OpenMP level is analyzed for the largest basin in the simulation domain (Volga basin).

Model simulations have been conducted using Lomonosov-2 supercomputer [26], using nodes with Intel Haswell-EP E5-2697v3, 2.6 GHz, 14 cores and Infiniband FDR interconnect. The executable of the land surface model was assembled with ifort compiler using -O3 optimization. In MPI series of runs, the model was launched as:

```
sbatch --ntasks=<number of MPI processes> --bind-to none <executable>
```

whereas for OpenMP series:

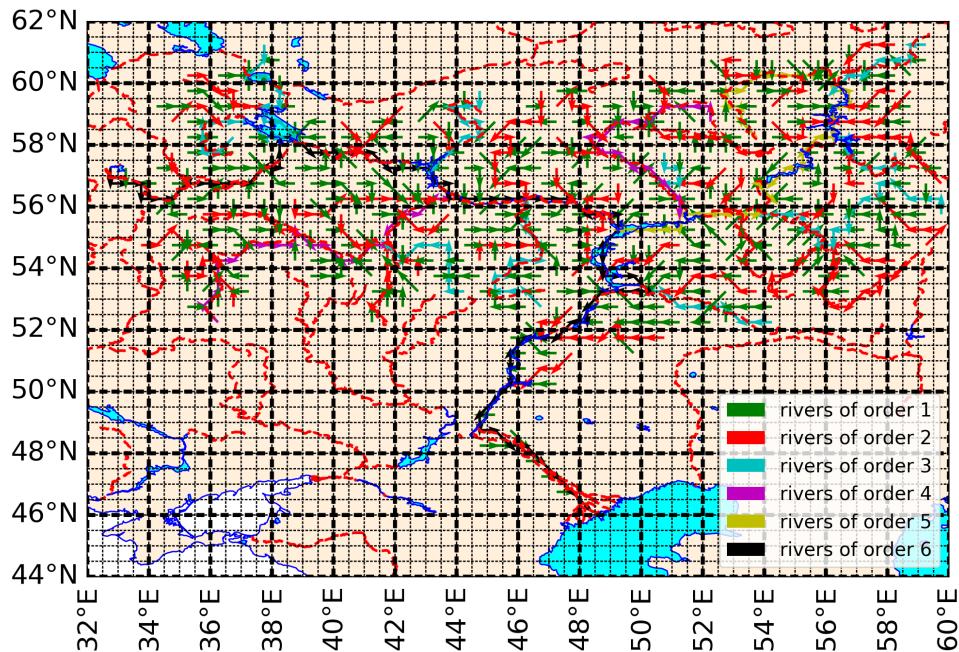


**Figure 5.** Volga river basin on the INM RAS-MSU model mesh (a subdomain of the full model domain shown in Fig. 4), each arrow denotes the river course segment containing mesh nodes depicted in Fig. 2, black thin dotted lines are used to show model cells, thick dashed black lines delineate MPI subdomains, color is used to denote the river Strahler order

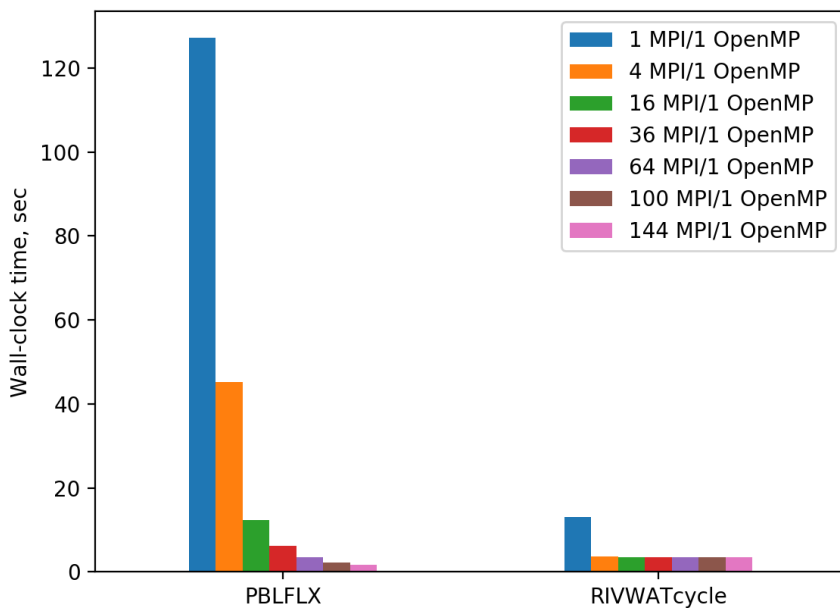
```
sbatch --ntasks=4 --ntasks-per-node=1 --bind-to none <executable>
```

The latter ensures that each MPI process runs at a separate node, and all OpenMP threads of a given MPI process locate at the same node.

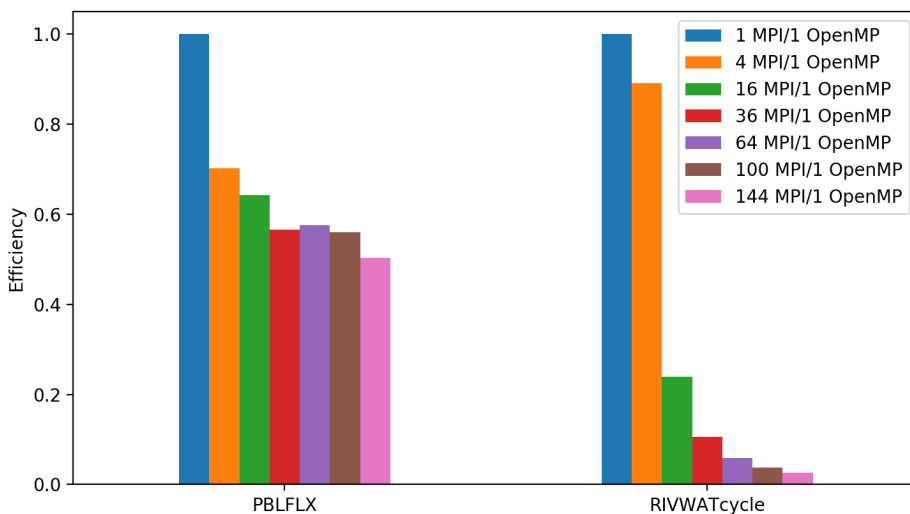
## 5. Results and Discussion

The wall-clock time and parallel efficiency (defined as the speedup of parallel version in respect to serial code version divided by number of MPI processes) for experiments of MPI series are shown in Fig. 6a and 6b, respectively.

The soil model accelerates with gradual decrease of efficiency from 0.79 at 4 cores to 0.52 at 144 cores, despite the absence of MPI exchanges in this part of the code. The reason is the load imbalance between MPI processes, taking into account that the wall-clock time of the soil model at any timestep is defined by the maximal wall-clock time among processes. At 4 cores, all MPI subdomains include ocean cells and different number of land cells which define the distribution of workload between processes. At large numbers of  $M_\phi M_\lambda$  there are subdomains with all cells residing over ocean, which means corresponding MPI processes are idle. The fraction of such processes is estimated as a fraction of ocean cells which is 30%. The efficiency may be corrected for this factor by taking into account only number of MPI processes, processing land cells, e.g. for 144 cores we have the corrected efficiency  $0.52/(1 - 0.3) = 0.74$ . The remaining loss of efficiency  $1 - 0.74 = 0.26$  is mostly explained by the increase of the time for one-timestep processing of a single soil column, averaged over a subdomain of the most loaded MPI-process, with rise of the cores number (from  $3.9 \times 10^{-5}$  s at 1 MPI process to  $4.9 \times 10^{-5}$  s at 144 MPI processes).



(a) Wall-clock time



(b) Parallel efficiency

**Figure 6.** Wall-clock time and parallel efficiency of the soil model (subroutine PBLFLX) and the river model (subroutine RIVWATcycle) using 1–144 MPI processes on Lomonosov-2 supercomputer (MPI series)

This means that even fully terrestrial MPI subdomains have different workload depending on the presence of snow cover and different number of iterations for surface temperature to perform a timestep depending on the local meteorological conditions.

The regular longitude-latitude decomposition of the LSM computational domain between MPI processes is inherited from the fully coupled ESM, where this decomposition matches the decomposition in the atmospheric model. However, as shown above, in standalone mode it be-

comes non-optimal if rectangular domain in  $(\lambda, \phi)$  contains ocean cells. In this case, the current MPI decomposition scheme can be optimized, in order the MPI subdomains to contain only land cells or a minimal number of ocean cells. This model improvement is left for the future.

Remarkably, the river model is accelerated almost 4 times when using 4 MPI processes, whereas under larger number of cores the wall-clock time remains almost constant. This is due to fact that at the MPI level, the largest river basin in the domain (Volga basin) is processed by single process, and the wall-clock time of this process is a minimal possible for the river model in general. As a result, the river model contribution to the whole land surface model runtime, being negligible in serial mode starts to dominate over the soil model above  $\sim 100$  MPI processes (3.49 s for river model vs. 1.75 s for soil model).

The time for ALLREDUCE operation gathering the data for the river model input gradually increases from 0.22 s at  $M_\phi M_\lambda = 4$  to 0.66 s at  $M_\phi M_\lambda = 144$  indicating increasing overhead costs of this collective operation, still remaining much less than river model computational time (3.49 s).

The wall-clock time and parallel efficiency of Volga basin processing in experiments of OpenMP series are shown in Fig. 7a and 7b, respectively. The efficiency is defined here in respect to the model configuration with 4 MPI processes and 1 OpenMP thread.

Simulation of rivers with smallest order demonstrated the highest speedup and efficiency, whereas the rivers of order 5 and 6 are simulated with no acceleration. The overall decrease of Volga simulation time when using 14 threads is 4.11 times which is much smaller compared to estimated  $\approx 12$  times from theoretical formula (24). To address this difference, consider the Volga basin scale-similarity parameters (Horton metrics) computed on the model mesh (Fig. 5), presented in Tab. 1.

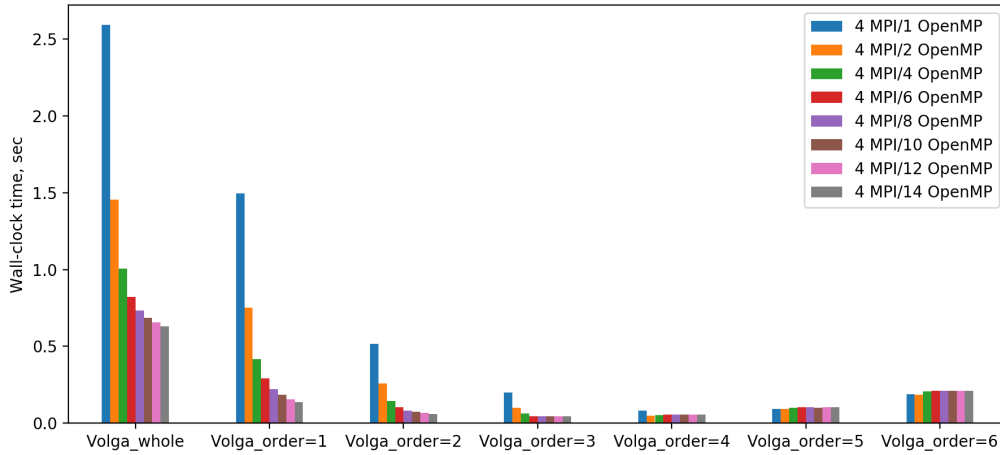
**Table 1.** The Horton metrics for Volga basin at  $0.5^\circ \times 0.5^\circ$

Horton parameter / Strahler order	$\omega = 2$	$\omega = 3$	$\omega = 4$	$\omega = 5$	$\omega = 6$
$C_{n,\omega}$	5.911	4.5	5	2	1
$C_{L,\omega}^*$	9.098	2.293	2.188	1.943	1.971

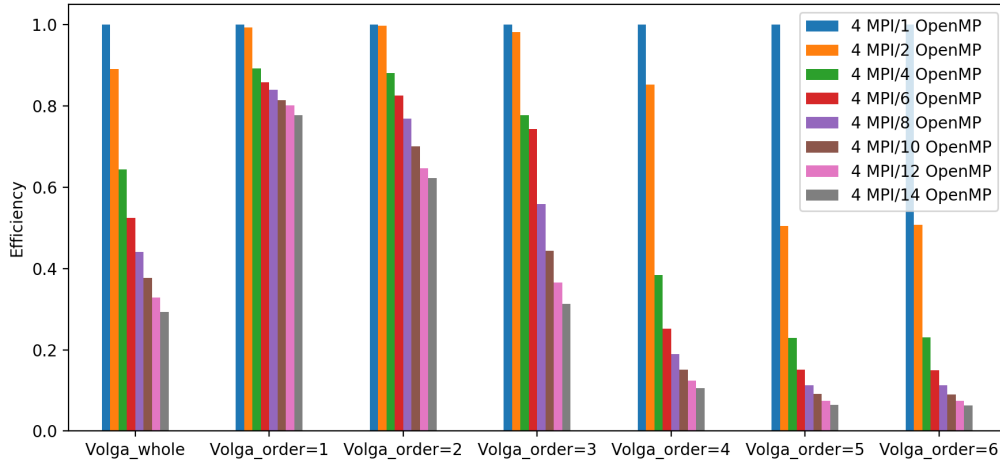
The river length parameter  $C_{L,\omega}^*$  is close to typical value of 2, excluding the case of  $\omega = 2$ , because the lengths of low-order rivers are not explicitly reproduced on the model mesh (e.g., the majority of first-order rivers have length of the one model cell). On the contrary, the river number parameter  $C_{n,\omega}$  is biased from typical value of  $\sim 4$  for the largest order 5 and 6. The value  $C_{n,6} = 1$  means that there are one river of order 5 and one river of order 6, which are both simulated sequentially by one OpenMP thread (see no speedup for those rivers in Fig. 7a). There are two rivers of order 4, so that the acceleration of their simulation ceases with the number of threads  $> 2$ . Gradual decrease of parallel efficiency of simulation of the rivers with orders 1 and 2 while increasing number of threads is caused by increasing the contribution of overheads of initializing the OpenMP PARALLEL section and DO loop each timestep to the total wall-clock time.

To check the reasoning of the previous paragraph, the formula (24) can be extended to account for variability of Horton coefficients with river order  $\omega$ :

$$\frac{T_s}{T_p} = \frac{n_1 \left[ 1 + \sum_{\omega=1}^{\omega_{max}-1} (c_{n,\omega+1} * c_{L,\omega+1}) \right]}{\max [n_1/m, 1] + \sum_{\omega=1}^{\omega_{max}-1} (\max [c_{n,\omega+1} * n_1/m, 1] * c_{L,\omega+1})}, \quad (25)$$



(a) Wall-clock time



(b) Parallel efficiency

**Figure 7.** Wall-clock time and parallel efficiency of the river model for Volga basin using 4 MPI processes and 1–14 OpenMP threads on Lomonosov-2 supercomputer; the metrics are given for the whole basin (“Volga\_whole”) and for groups of rivers having the same order (“Volga\_order=<n>”) (OpenMP series)

where  $c_{n,\omega} \doteq \prod_{i=2}^{\omega} C_{n,i}^{-1}$  and  $c_{L,\omega} \doteq \prod_{i=2}^{\omega} C_{L,i}^{*k}$ . Substituting to (25) the values from Tab. 1 provides  $T_s/T_p = 3.28$  for 14 OpenMP nodes, which is much closer to measured acceleration 4.11 compared to that given by formula (24) with reference Horton metrics ( $\approx 12$  times). The real acceleration appears to be faster, as the expression (25) does not take into account overheads for processing each river, related to invoking subroutines, allocating memory etc. In serial mode, these overheads increase especially the total wall-clock time for solution of model equations for small-order rivers (due to their large number), and since parallelization of these river orders is more efficient, this improves the parallel performance for the whole basin.

To summarize, processing of the Volga basin is significantly accelerated up to 4–6 OpenMP threads, this limit taking place due to serial processing of longest rivers of order 5 and 6. However, with finer meshes of land surface models, which are expected in future, the orders of resolved

large river basins are to increase and thus the efficiency OpenMP-based approach presented here is anticipated to improve, according to estimates presented in Section 3.

## Conclusion

This paper presents a new version of the INM RAS-MSU land surface scheme where the river hydrodynamic and thermodynamic model is embedded into the parallel execution framework using two levels of parallelism: the first is MPI-based independent processing of river basins, and the second uses OpenMP technique to parallelize the simulation of rivers of the same Strahler order. Numerical experiments have been performed for the East European domain with resolution  $0.5^\circ \times 0.5^\circ$ . The MPI implementation of the soil model is based on conventional even longitude-latitude decomposition of the model domain, inherited from the atmospheric model. The soil model parallel efficiency at 1–144 cores was shown to be 0.52–0.79 and limited by the presence of ocean area, and by imbalance of computational load between soil columns depending on the presence of snow cover and number of iterations for the surface temperature needed to advance the soil profiles. The acceleration of the river model at MPI level (not exceeding 4 times) is defined by the size of the largest river basin in the domain (Volga), whereas at OpenMP level the potential for acceleration of large river basin simulation is shown to be close to number of threads used. OpenMP-level speedup was hindered in our numerical experiments by the underestimation of river orders at coarse land surface model resolution (recommended performance for the Volga basin attained at 4–6 threads with 2.5–3 times acceleration).

The future development of the parallel code includes MPI+OpenMP implementation of the soil model, optimization of MPI domain decomposition for soil model under presence of ocean surface, and further tuning the MPI+OpenMP configuration of the river model.

## Acknowledgements

The work is partially supported by the Russian Ministry of Science and Higher Education (agreement No. 075-15-2019-1621, MPI implementation of the soil model), by the Russian Science Foundation (project No. 21-71-30003, MPI+OpenMP implementation of the river model), and the Russian Foundation for Basic Research (project No. 20-05-00773, configuration of numerical experiments, preparation of the input data). The research is carried out using the equipment of the shared research facilities of HPC computing resources at Lomonosov Moscow State University.

*This paper is distributed under the terms of the Creative Commons Attribution-Non Commercial 3.0 License which permits non-commercial use, reproduction and distribution of the work without further permission provided the original work is properly cited.*

## References

1. Bell, V.A., Kay, A.L., Jones, R.G., Moore, R.J.: Development of a high resolution grid-based river flow model for use with regional climate model output. *Hydrology and Earth System Sciences* 11(1), 532–549 (2007). <https://doi.org/10.5194/hess-11-532-2007>
2. Bowring, S.P.K., Lauerwald, R., Guenet, B., et al.: ORCHIDEE MICT-LEAK (r5459), a global model for the production, transport, and transformation of dissolved organic carbon from Arctic permafrost regions – Part 1: Rationale, model description, and simulation proto-

- col. *Geoscientific Model Development* 12(8), 3503–3521 (2019). <https://doi.org/10.5194/gmd-12-3503-2019>
3. Bowring, S.P.K., Lauerwald, R., Guenet, B., et al.: ORCHIDEE MICT-LEAK (r5459), a global model for the production, transport, and transformation of dissolved organic carbon from Arctic permafrost regions – Part 2: Model evaluation over the Lena River basin. *Geoscientific Model Development* 13(2), 507–520 (2020). <https://doi.org/10.5194/gmd-13-507-2020>
  4. Brooks, R., Corey, A.: *Hydraulic Properties of Porous Media*. Tech. rep., Colorado State University, Fort Collins (1964)
  5. Clapp, R., Hornberger, M.: Empirical equations for some soil hydraulic properties. *Water Resources Research* 14(4), 601–604 (1978)
  6. Conil, S., Douville, H., Tyteca, S.: The relative influence of soil moisture and SST in climate predictability explored within ensembles of AMIP type experiments. *Climate Dynamics* 28(2), 125–145 (2007). <https://doi.org/10.1007/s00382-006-0172-2>
  7. Döll, P., Lehner, B.: Validation of a new global 30-min drainage direction map. *Journal of Hydrology* 258(1-4), 214–231 (2002). [https://doi.org/10.1016/S0022-1694\(01\)00565-0](https://doi.org/10.1016/S0022-1694(01)00565-0)
  8. Downing, J., Cole, J., Duarte, C., et al.: Global abundance and size distribution of streams and rivers. *Inland Waters* 2(4), 229–236 (2012). <https://doi.org/10.5268/IW-2.4.502>
  9. Du, C.: Comparison of the performance of 22 models describing soil water retention curves from saturation to oven dryness. *Vadose Zone Journal* 19(1) (2020). <https://doi.org/10.1002/vzj2.20072>
  10. Fadeev, R.Y., Ushakov, K.V., Tolstykh, M.A., Ibrayev, R.A.: Design and development of the SLAV-INMIO-CICE coupled model for seasonal prediction and climate research. *Russian Journal of Numerical Analysis and Mathematical Modelling* 33(6), 333–340 (2018). <https://doi.org/10.1515/rnam-2018-0028>
  11. Falloon, P., Betts, R., Bunton, C.: *New Global River Routing Scheme in the Unified Model*. Tech. rep., Hadley Centre (2007)
  12. van Genuchten, M.T.: A Closed-form Equation for Predicting the Hydraulic Conductivity of Unsaturated Soils. *Soil Science Society of America Journal* 44(5), 892–898 (1980). <https://doi.org/10.2136/sssaj1980.03615995004400050002x>
  13. Guth, P.L.: Drainage basin morphometry: a global snapshot from the shuttle radar topography mission. *Hydrology and Earth System Sciences* 15(7), 2091–2099 (2011). <https://doi.org/10.5194/hess-15-2091-2011>
  14. Huang, B., Mehta, V.M.: Influences of freshwater from major rivers on global ocean circulation and temperatures in the MIT ocean general circulation model. *Advances in Atmospheric Sciences* 27(3), 455–468 (2010). <https://doi.org/10.1007/s00376-009-9022-6>
  15. Lucas-Picher, P., Arora, V.K., Caya, D., Laprise, R.: Implementation of a large-scale variable velocity river flow routing algorithm in the Canadian Regional Climate Model (CRCM). *Atmosphere-Ocean* 41(2), 139–153 (2003). <https://doi.org/10.3137/ao.410203>

16. Lykossov, V., Palagin, E.: Dynamics of coupled heat and moisture transport in the soil-atmosphere system. *Russian Meteorology and Hydrology* 8, 48–56 (1978), (in Russian)
17. Malakhova, V., Golubeva, E.: The role of the Siberian rivers in increasing dissolved methane in the East Siberian shelf. *Bull. Nov. Comp. Center, Num. Model. in Atmosph.* 13, 43–56 (2014)
18. Medvedev, A.I., Stepanenko, V.M.: The influence of external parameters on river runoff in the INM RAS – MSU land surface model. *IOP Conference Series: Earth and Environmental Science* 611, 012023 (2020). <https://doi.org/10.1088/1755-1315/611/1/012023>
19. Miralles, D.G., Teuling, A.J., van Heerwaarden, C.C., Vilà-Guerau de Arellano, J.: Mega-heatwave temperatures due to combined soil desiccation and atmospheric heat accumulation. *Nature Geoscience* 7(5), 345–349 (2014). <https://doi.org/10.1038/ngeo2141>
20. Mualem, Y.: A new model for predicting the hydraulic conductivity of unsaturated porous media. *Water Resources Research* 12(3), 513–522 (1976). <https://doi.org/10.1029/WR012i003p00513>
21. Raymond, P.A., Hartmann, J., Lauerwald, R., et al.: Global carbon dioxide emissions from inland waters. *Nature* 503(7476), 355–359 (2013). <https://doi.org/10.1038/nature12760>
22. Sheng, M., Lei, H., Jiao, Y., Yang, D.: Evaluation of the Runoff and River Routing Schemes in the Community Land Model of the Yellow River Basin. *Journal of Advances in Modeling Earth Systems* 9(8), 2993–3018 (2017). <https://doi.org/10.1002/2017MS001026>
23. Solomon, A., Heuzé, C., Rabe, B., et al.: Freshwater in the Arctic Ocean 2010–2019. *Ocean Science* 17(4), 1081–1102 (2021). <https://doi.org/10.5194/os-17-1081-2021>
24. Stepanenko, V., Medvedev, A., Korpushenkov, I., et al.: A River Routing Scheme for an Earth System Model. *Numerical Methods and Programming* 20, 396–410 (2019). <https://doi.org/10.26089/NumMet.v20r435>, (in Russian)
25. Tarboton, D.G., Bras, R.L., Rodriguez-Iturbe, I.: The fractal nature of river networks. *Water Resources Research* 24(8), 1317–1322 (1988). <https://doi.org/10.1029/WR024i008p01317>
26. Voevodin, V.V., Antonov, A.S., Nikitenko, D.A., et al.: Supercomputer Lomonosov-2: Large Scale, Deep Monitoring and Fine Analytics for the User Community. *Supercomputing Frontiers and Innovations* 6(2), 4–11 (2019). <https://doi.org/10.14529/jsfi190201>
27. Volodin, E.M., Gritsun, A.S.: Simulation of Possible Future Climate Changes in the 21st Century in the INM-CM5 Climate Model. *Izvestiya, Atmospheric and Oceanic Physics* 56(3), 218–228 (2020). <https://doi.org/10.1134/S0001433820030123>
28. Volodina, E., Bengtsson, L., Lykossov, V.N.: Parameterization of heat and moisture transfer in a snow cover for modelling of seasonal variations of land hydrological cycle. *Russian Journal of Meteorology and Hydrology* (5), 5–14 (2000)
29. Vorobyev, S.N., Karlsson, J., Kolesnichenko, Y.Y., et al.: Fluvial carbon dioxide emission from the Lena River basin during the spring flood. *Biogeosciences* 18(17), 4919–4936 (2021). <https://doi.org/10.5194/bg-18-4919-2021>

30. Vreman, A.W.: The adjoint filter operator in large-eddy simulation of turbulent flow. *Physics of Fluids* 16(6), 2012–2022 (2004). <https://doi.org/10.1063/1.1710479>
31. Ye, A., Duan, Q., Zhan, C., et al.: Improving kinematic wave routing scheme in Community Land Model. *Hydrology Research* 44(5), 886–903 (2013). <https://doi.org/10.2166/nh.2012.145>
32. Zhang, H., Liu, J., Li, H., et al.: The Impacts of Soil Moisture Initialization on the Forecasts of Weather Research and Forecasting Model: A Case Study in Xinjiang, China. *Water* 12(7), 1892 (2020). <https://doi.org/10.3390/w12071892>